IOPscience iopscience.iop.org

Home Search Collections Journals About Contact us My IOPscience

Ternary clathrates Ba–Cd–Ge: phase equilibria, crystal chemistry and physical properties

This article has been downloaded from IOPscience. Please scroll down to see the full text article.

2007 J. Phys.: Condens. Matter 19 046203

(http://iopscience.iop.org/0953-8984/19/4/046203)

View the table of contents for this issue, or go to the journal homepage for more

Download details:
IP Address: 129.252.86.83
The article was downloaded on 28/05/2010 at 15:55

Please note that terms and conditions apply.

INSTITUTE OF PHYSICS PUBLISHING JOURNAL OF PHYSICS: CONDENSED MATTER

J. Phys.: Condens. Matter **19** (2007) 046203 (23pp) doi:10.1088/0953-8984/19/4/046203

Ternary clathrates Ba–Cd–Ge: phase equilibria, crystal chemistry and physical properties

N Melnychenko-Koblyuk[1], A Grytsiv[1], St Berger[1], H Kaldarar[2], H Michor[2], F Röhrbacher[2], E Royanian[1,2], E Bauer[2], P Rogl[1,4], H Schmid[1] and G Giester[3]

[1] Institut für Physikalische Chemie, University of Vienna, A-1090 Vienna, Währingerstrasse 42, Austria
[2] Institut für Festkörperphysik, TU Wien, A-1040 Wien, Wiedner Hauptstrasse 8-10, Austria
[3] Institut für Mineralogie und Kristallographie, University of Vienna, A-1090 Vienna, Althanstrasse 14, Austria

E-mail: peter.franz.rogl@univie.ac.at

Received 1 August 2006, in final form 27 November 2006
Published 12 January 2007
Online at stacks.iop.org/JPhysCM/19/046203

Abstract

The present paper describes the formation, phase relations at subsolidus temperatures and at 800 °C, crystal chemistry and physical properties of a series of ternary clathrates as part of the solid solution $Ba_8Cd_xGe_{43-5x/8}\square_{3-3x/8}$, derived from binary $Ba_8Ge_{43}\square_3$ with a solubility limit of 8 Cd per formula unit at 800 °C. Structural investigations in all cases confirm cubic primitive symmetry with a lattice parameter $a \approx 1.1$ nm, consistent with the space group type $Pm\bar{3}n$. Both the temperature dependent x-ray spectra and the heat capacity define a low-lying, almost localized, phonon branch.

Studies of transport properties show electrons to be the majority charge carriers in the systems. As the Cd content increases, the system is driven towards a metal-to-insulator transition, causing $Ba_8Cd_{4.7}Ge_{40.3}\square_{1.0}$, for example, to show metallic behaviour at low temperatures while at high temperatures semiconducting features become obvious. A model based on a gap of the electronic density of states slightly above the Fermi energy perfectly explains such a scenario. Thermal conductivity exhibits a pronounced low temperature maximum, dominated by the lattice contribution, while at higher temperatures the electronic part becomes more important.

(Some figures in this article are in colour only in the electronic version)

Dedicated to Professor Hans Georg von Schnering on the occasion of his 75th birthday

[4] Author to whom any correspondence should be addressed.

 © 2007 IOP Publishing Ltd Printed in the UK

1. Introduction

In order to raise the efficiency of thermoelectric cooling devices, in 1995 Glen Slack proposed the PGEC (phonon glass and electron crystal) concept for novel thermoelectric materials, which should combine the properties required for good electric conductivity of a crystal with the poor thermal conductivity of a glass [1]. This idea was realized in compounds with a rigid structure, responsible for the electrical conductivity, and by heavy atoms rattling in large cages, thereby ensuring low thermal conductivity via additional scattering of the phonons [2]. A new approach applies to clathrate phases with an extended three-dimensional framework of germanium or silicon atoms, providing huge voids usually filled by large electropositive elements, R = Na, K, Cs, Rb, Sr, Ba, Eu. Taking into account that some d and p elements are necessary for stabilization of the framework structure as well as for proper adjustment of the electronic structure, the objects of this investigation are the ternary clathrate phases $Ba_8Cd_xGe_{46-x}$ and $Ba_6Cd_xGe_{25-x}$. In a simple model, the electronic structure of clathrates can be understood in terms of the Zintl concept: binary $Ba_8Ge_{43}\square_3$ with three framework defects [3, 4] can thus be formulated as $[Ba^{+2}]_8[Ge^0]_{43}[\square^{-4}]_3$ yielding four electrons as carriers per formula unit. Substitution and doping are therefore a fruitful tools for tuning the charge carrier concentration of clathrates in an optimal manner to tailor the highest possible thermoelectric performance. Interest has hitherto been mainly devoted to investigations of the thermoelectric properties of type I clathrates $R_8M_xGe_{46-x}$ (M is Ga, In, Cu and Ni), whereas only limited information is available on the thermoelectric performance of clathrates stabilized by other transition metals, such as Cd.

Earlier investigations [5] and [6] reported on the crystal structure of type I clathrates '$Ba_8Cd_xGe_{46-x}$'. Whilst [5, 6] defined the structure of $Ba_8Cd_8Ge_{38}$ from single crystal data, the authors of [6] listed $Ba_8Cd_8Ge_{38}$ as the limit of the compositional range. Two vacancies were found for the composition $Ba_8Cd_4Ge_{40}\square_2$ [6]. However, no data were presented for small Cd concentrations and no link was made to the binary clathrates Ba_8Ge_{43} [4] and Ba_6Ge_{25} [7]. Furthermore, no physical properties of ternary Ba–Cd–Ge compounds are available in the literature.

Therefore the tasks of the present work are: (a) to establish the extension of the clathrate single-phase regions in the ternary system Ba–Cd–Ge, (b) to elucidate details of the crystal structure of clathrate type I, (c) to construct a phase diagram in the Ba–Cd–Ge system at 800 °C and (d) to investigate the physical (transport) properties of the ternary Cd-based clathrates.

2. Experimental details

Alloys with a weight of 2 g were prepared from elemental ingots (Ba 99.9, Cd 99.99 and Ge 99.999 mass%) by melting in sealed quartz tubes at 1000 °C for 2 h. Afterwards samples were furnace cooled to 800 °C and annealed at this temperature for 4–7 days prior to quenching in cold water.

Single crystals were mechanically isolated from crushed alloys. Inspection on an AXS-GADDS texture goniometer ensured high crystal quality, unit cell dimensions and Laue symmetry of the specimens prior to collection of x-ray intensity data on a four-circle Nonius Kappa diffractometer equipped with a CCD area detector employing graphite monochromatic Mo Kα radiation (λ = 0.071 073 nm). The orientation matrix and unit cell parameters for a cubic system were derived using the program DENZO [8]. No absorption corrections were necessary because of the rather regular crystal shape and small dimensions of the investigated specimens. The structures were refined with the aid of the SHELXL-97 program [9]. X-ray intensity data for a single crystal with composition $Ba_8Cd_{7.6}Ge_{38.4}$ were collected at three

temperatures, 100, 200 and 300 K, and isothermal temperatures for the crystal, mounted with transparent varnish on a glass rod, were ensured by a continuous stream of nitrogen gas enclosing the crystal at the preset temperature.

X-ray powder diffraction (XPD) data from alloys were collected employing a Guinier–Huber image plate system with Cu Kα_1 radiation ($8° < 2\theta < 100°$). Precise lattice parameters were calculated by least-squares fits to the indexed θ values employing Ge as an internal standard ($a_{Ge} = 0.565\,7906$ nm). Quantitative Rietveld refinements of the x-ray powder diffraction data were performed with the FULLPROF program [10], with the use of its internal tables for scattering lengths and atomic form factors.

The as-cast and annealed samples were polished using standard procedures and were examined by optical metallography and scanning electron microscopy (SEM). Compositions were determined via electron probe micro-analyses (EPMA) on a Carl Zeiss DSM 962 equipped with a Link EDX system operated at 20 kV and 60 μA. Compounds Ba_8Ge_{43} and Ba_6Ge_{25} were used as EPMA standards.

Samples for physical property measurements were all examined by LOM, SEM, EPMA and only specimens with secondary phases (typically Ge) amounting to less than 2 vol% were used. To physically characterize the samples, we have investigated the temperature dependent resistivity, thermal conductivity, specific heat and Seebeck coefficient. Thermopower measurements were carried out employing a differential method. The absolute thermopower $S_x(T)$ was calculated using the following equation: $S_x(T) = S_{Pb}(T) - V_{Pb}/x/\Delta T$, where S_{Pb} is the absolute thermopower of lead and V_{Pb}/x is the thermally induced voltage across the sample, depending on the temperature difference ΔT. While the temperature dependent resistivity was measured in a standard four-terminal dc technique, thermal conductivity below room temperature was obtained by a steady state heat flow method on rectangular shaped samples with a typical cross section of 1–2 mm^2 and a length of about 10 mm. The temperature gradient along the sample was determined by a differential Au/0.07% Fe versus Chromel thermocouple and the absolute temperature was measured by a Ge resistor below 40 K and a Pt resistor in the range from 40 to 300 K, respectively. Three concentric radiation shields were mounted around the sample. Specific heat measurements were carried out on samples of about 1 g in the temperature range 1.5–140 K employing a quasi adiabatic step heating technique. Temperature was obtained from a calibrated CERNOX resistor; heat capacity data were calibrated against high purity Cu.

3. Results and discussion

3.1. Phase equilibria in the Ge-rich region of Ba–Cd–Ge

With respect to crystallographic data available in literature on Cd-stabilized clathrate type I, one task of the present work was to determine the full range of the ternary clathrate solution extending from binary $Ba_8Ge_{43}\square_3$ (the $\square$ indicates a defect). With increase of Cd, EPMA data clearly reveal a decrease of the Ba content (table 1) associated with a change in the number of vacancies in the crystal lattice.

Vacancies in the framework of the structure were calculated from EPMA data assuming a complete Ba sublattice (2a and 6d sites). The number of vacancies decreases almost linearly with increasing Cd content (figure 1) and vanishes for the composition with eight atoms of Cd per formula unit.

This composition constitutes the solubility limit of Cd in type I clathrate at 800 °C. The number of vacancies as a function of the Cd content is compared for two boundary models of incorporation of Cd atoms into the $Ba_8Ge_{43}\square_3$ lattice. *Model A* corresponds to Cd/Ge

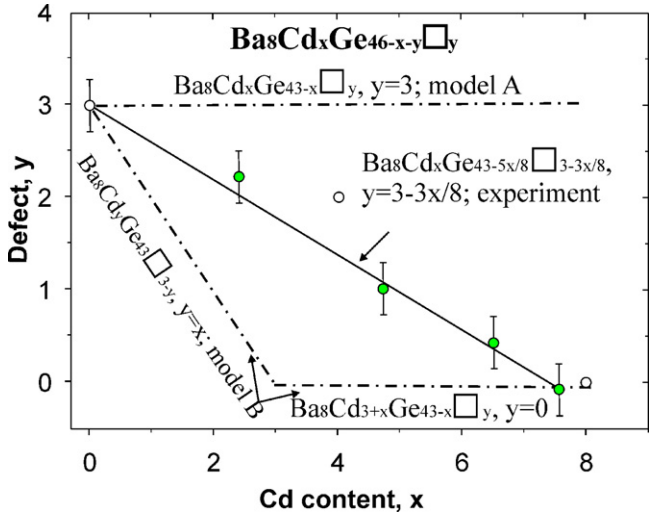

Figure 1. Vacancy (y) in clathrate type I $Ba_8Cd_xGe_{46-x-y}\square_y$ versus Cd content (x). Filled symbols, this work; open symbols, [3] for Ba_8Ge_{43} and [6] for ternary compositions.

Table 1. Composition (EPMA) and lattice parameter for $Ba_8Cd_xGe_{43-5x/8}\square_{3-3x/8}$.

Nominal composition	Composition from EPMA, (at.%)			Formula[a] from EPMA			Accepted composition	Lattice parameter a (nm)
	Ba	Cd	Ge	Cd	Ge	□		
Ba_8Ge_{43}	15.69	0.00	84.31	0.00	43.00	3.00	$Ba_8Ge_{43}\square_3$	1.065 7(2)
$Ba_8Cd_2Ge_{44}$	15.45	4.65	79.90	2.41	41.36	2.23	$Ba_8Cd_{2.4}Ge_{41.4}\square_{2.2}$	1.075 18(3)
$Ba_8Cd_4Ge_{42}$	15.10	8.92	75.98	4.73	40.26	1.02	$Ba_8Cd_{4.7}Ge_{40.3}\square_{1.0}$	1.085 00(2)
$Ba_8Cd_6Ge_{40}$	14.93	12.15	72.92	6.51	39.06	0.43	$Ba_8Cd_{6.5}Ge_{39.1}\square_{0.4}$	1.091 90(2)
$Ba_8Cd_8Ge_{38}$	14.79	13.98	71.22	7.56	38.51	−0.07	$Ba_8Cd_{7.6}Ge_{38.4}$	1.094 99(3)

[a] Ba sublattice (2a and 6d sites) was found to be complete.

substitution at a constant level of vacancies (three voids per formula as observed in binary $Ba_8Ge_{43}\square_3$). Accordingly the composition is described by the formula $Ba_8(Cd_xGe_{43-x})\square_3$. *Model B* suggests that Cd atoms first enter the three empty lattice sites and only after completely filling these sites at $x = 3$ do Cd atoms start to substitute for Ge following the formula $Ba_8(Cd_{3+x}Ge_{43-x})$. Experimental data clearly show a behaviour intermediate between these two models, i.e. Cd atoms fill vacancies and simultaneously substitute for Ge atoms in the framework. Although $Ba_8Cd_xGe_{46-x-y}\square_y$ arises as a general formula, the almost linear behaviour ($y = 3 - 3x/8$, figure 1) defines the detailed formula $Ba_8Cd_xGe_{43-5x/8}\square_{3-3x/8}$ ($0 < x < 8$). The composition dependence of the lattice parameters for $Ba_8Cd_xGe_{46-x-y}\square_y$ is shown in figure 2 and compares well with available literature data.

The increase of the unit cell parameters with Cd content is in line with the difference in the atomic radii of the elements. The sample $Ba_8Cd_8Ge_{38}$ (nominal composition) is a single-phase clathrate with lattice parameter $a = 1.094\,99(3)$ nm, but ternary alloys with higher Cd content were found to be multiphase with a similar lattice parameter for the clathrate phase. Thus the solubility limit at 800 °C corresponds to the composition $Ba_8Cd_{8.02}G_{37.98}$ ($a = 1.096\,12(3)$ nm).

In order to evaluate the long-term stability of the clathrate phase at low temperature a sample with nominal composition $Ba_8Cd_8G_{38}$ was annealed at 500 °C for 5 months. X-ray

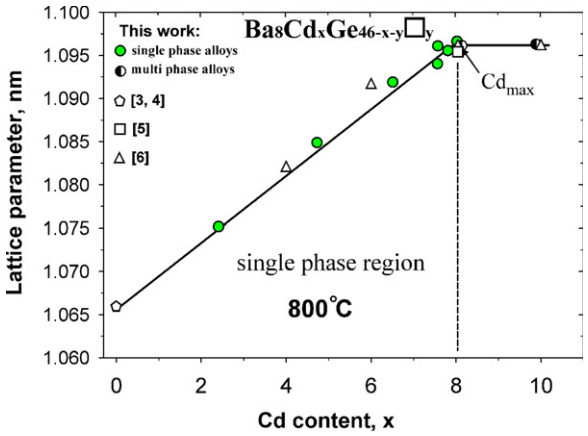

Figure 2. Lattice parameters versus Cd content for $Ba_8Cd_xGe_{46-x-y}\square_y$ alloys. The dashed line denotes the solubility limit of Cd at 800 °C.

powder diffraction still reveals a single-phase clathrate pattern with lattice parameter $a = 1.096\,10(2)$ nm, indicating a composition identical to the as-cast state and annealed state at 800 °C. With respect to the small temperature range of existence for Ba_8Ge_{43} from 770 to 810 °C [4] we observe a significant increase of thermodynamic stability for the Cd-based clathrate.

Alloys containing $BaGe_2$ are moisture sensitive and quickly decompose. This provokes significant difficulties in specimen preparation (EPMA and LOM) and x-ray powder diffraction profiles turn complicated, due to formation of various decomposition products and/or hydrolysis of $BaGe_2$. In order to establish the composition of both clathrate I and clathrate IX in equilibrium with $BaGe_2$, the decomposed alloy $Ba_6Cd_2Ge_{23}$ was washed in diluted H_2SO_4 from decomposition products (brown powder) finally yielding a metallic powder. XPD indeed shows that the residue consists of a mixture of two clathrates (type I and IX). The lattice parameter for clathrate IX ($a = 1.455\,65(4)$ nm) is close to that for binary Ba_8Ge_{25} ($a = 1.455\,63(3)$ nm, our data, and $a = 1.455\,64(2)$ nm after [7]) and reveals only limited solubility of Cd, which was estimated to be less than 0.2 at.%. Clathrate type I has a lattice parameter $a = 1.088\,10(3)$ nm. This value on the lattice parameter versus Cd concentration curve indicates a composition of $Ba_8Cd_{5.7}Ge_{39.7}\square_{0.6}$ for the clathrate type I solution (see figure 2).

During investigation of phase equilibria a new ternary compound with composition $BaCd_2Ge_2$ ($BaAl_4$ derivative structure and sub-cell parameters $a = 0.467\,35(6)$ to $0.469\,14(4)$, $c = 1.1273(4)$ to $1.1453(6)$ nm) was found, which exhibits a small homogeneity region of about 2 at.% at 800 °C. Details of the crystal structure and its physical properties will be the subject of a forthcoming publication.

The available experimental data on the constitution of the alloys after annealing at 800 °C (table 2) provide the phase relations involving both clathrate phases. It has to be noted that at 800 °C some alloys are in equilibrium with a Cd-rich liquid phase that covers a significant part of the isothermal section (see figure 3(a)). The phase composition and state of the alloys after solidification (quenched from 800 °C) were used to define the subsolidus diagram of the system presented in figure 3(b).

Analysing the phase relations in the melting/crystallization region one can see that $Ba_8Cd_xGe_{43-5x/8}\square_{3-3x/8}$ (clathrate type I) coexists in equilibrium with all other phases at least in the investigated part of the system. Crystallization of clathrate I from liquid and annealing

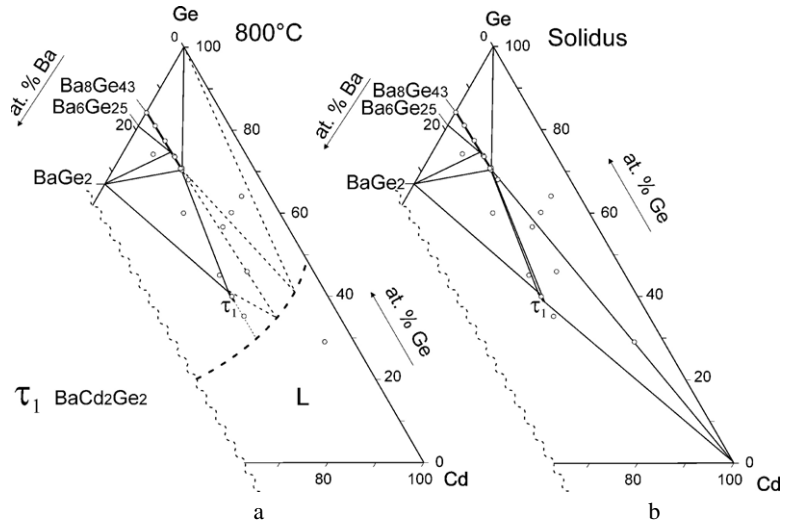

Figure 3. Ba–Cd–Ge ternary system for the region Cd–Ge–$BaGe_2$: isothermal section at 800 °C (a) and at solidus temperatures (b).

Table 2. EPMA and crystallographic data for selected Ba–Cd–Ge alloys annealed at 800 °C.

			Lattice parameters (nm)		EPMA (at.%)		
Nominal composition	Phase analysis	Structure type	*a*	*c*	Ba	Cd	Ge
$Ba_{19.35}Cd_{6.45}Ge_{74.20}$[a]	$Ba_8Cd_{5.7}Ge_{39.7}\square_{0.6}$	K_4Ge_{25-x}	1.088 10(3)				
	$BaGe_2$	$BaSi_2$					
	Ba_6Ge_{25}	Ba_6Ge_{25}	1.455 63(3)				
$Ba_{20}Cd_{20}Ge_{60}$[a]	$Ba_8Cd_8Ge_{38}$	K_4Ge_{25-x}	1.096 09(2)				
	$BaCd_2Ge_2$	'$BaAl_4$'					
	$BaGe_2$	$BaSi_2$					
$Ba_{10}Cd_{30}Ge_{60}$	$Ba_8Cd_{8.01}Ge_{38}$	K_4Ge_{25-x}	1.094 73(2)		14.43	14.45	71.12
	Ge	C_{diam}	0.565 72(2)		—	—	100.0
	Eutectic				6.43	51.04	42.53
$Ba_{14}Cd_{40}Ge_{46}$	$Ba_8Cd_{7.79}Ge_{38}$	K_4Ge_{25-x}	1.095 02(3)		14.68	14.29	71.03
	$BaCd_2Ge_2$	'$BaAl_4$'			19.64	39.12	41.24
	Eutectic				13.75	52.13	34.12
$Ba_{20}Cd_{40}Ge_{40}$	$BaCd_2Ge_2$	'$BaAl_4$'	0.467 35(6)	1.144 8(11)			
$Ba_{20}Cd_{45}Ge_{35}$	$BaCd_2Ge_2$	'$BaAl_4$'	0.467 43(9)	1.145 3(6)	19.96	40.09	39.95
	Cd	Mg	0.297 74(3)	0.561 73(2)	—	100.0	—
	Eutectic				19.54	50.73	29.75

[a] Alloy was decomposed; x-ray data are from a specimen washed in dilute H_2SO_4.

at 800 °C leads to the formation of large single crystal specimens. X-ray inspection of the crystals (used for physical property measurements) on an AXS-GADDS texture goniometer shows the good quality of the diffraction spots and identical orientation matrices at various positions located along the sample within a total length of 2 cm, confirming a single crystal condition.

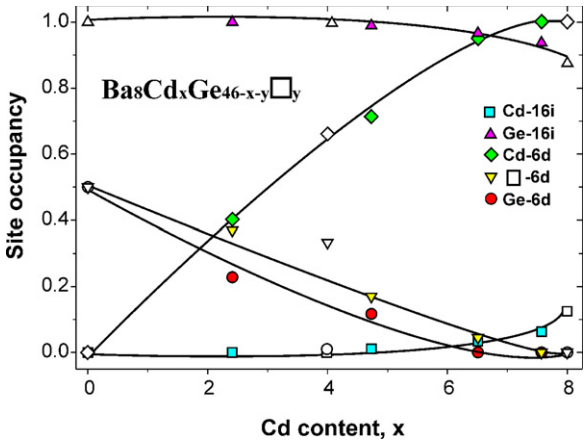

Figure 4. Site preference in $Ba_8Cd_xGe_{46-x-y}\square_y$. Filled symbols, this work; open symbols, [3] for Ba_8Ge_{43} and [6] for ternary compositions.

3.2. Crystal chemistry of $Ba_8Cd_xGe_{43-5x/8}\square_{3-3x/8}$

In order to evaluate atom site preferences in $Ba_8Cd_xGe_{43-5x/8}\square_{3-3x/8}$ x-ray diffraction data from single crystals with $x = 2.4$, 4.7, 6.5 and 7.6 were collected at room temperature. In all cases extinctions and diffraction intensities were consistent with a primitive cubic lattice (space group $Pm\bar{3}n$, $a \approx 1.1$ nm) and indicated isotypism with the structure of clathrate type I. No extra reflections indicating a larger unit cell $a' = 2a$ as reported by [4] for Ba_8Ge_{43} were detected in the investigated ternary crystals. First refinements were performed in order to determine trends in the variation of electron densities over the sites of the structure as a function of increasing Cd content. The heavy barium atoms were unambiguously found in sites 2a (0, 0, 0) and 6c (1/4, 0, 1/2), whilst the electron density distribution for the remaining sites appeared as follows: (i) constant electron densities of about 32e/atom in both lattice sites 16i and 24k, (ii) an increasing number of electrons in the 6d site from 16 e/atom for binary $Ba_8Ge_{43}\square_3$ (data of [4]) to ∼46 e/atom for $Ba_8Cd_{6.5}Ge_{39.1}\square_{0.4}$ and $Ba_8Cd_{7.6}Ge_{38.4}$ (figure 4). Consequently, the electron densities obtained reflect incorporation of Cd mainly into the 6d site of the $Ba_8Ge_{43}\square_3$ lattice. This site is partially occupied by Ge (50%) in $Ba_8Ge_{43}\square_3$ but is filled by Cd in $Ba_8Cd_xGe_{43-5x/8}\square_{3-3x/8}$ at $x \geqslant 6$. At lower x the 6d site contains Ge and Cd atoms as well as vacancies. With three species in one site (6d; Ge, Cd, vacancy) refinement was continued by inferring the practically linear variation of the vacancy concentration versus Cd content as derived from EPMA data (see figure 1), i.e. for each crystal the number of vacancies in the 6d site was taken from figure 1 as a fixed value. For compositions richer in Cd than six Cd atoms per unit cell, Cd atoms need to be considered in the 16i and/or 24k sites. With these constraints refinements were performed aiming at best agreement between refined composition and that obtained from EPMA as a main criterion of reliability (tables 3 and 4). For $Ba_8Cd_{7.6}Ge_{38.4}$ the 6d site was found to be fully occupied by Cd atoms, with a small fraction of additional Cd substituting Ge in the 16i sites (refinements reject any Cd in the 24k site). For $Ba_8Cd_{6.5}Ge_{39.1}\square_{0.4}$ the 6d site was found to be partially filled: 0.955Cd + 0.045□ with some Cd/Ge replacement in the 16i site revealing a composition of $Ba_8Cd_{6.2}Ge_{39.5}\square_{0.3}$ in fine agreement with EPMA data. Similarly, x-ray diffraction data for crystals with smaller Cd contents ($Ba_8Cd_{2.4}Ge_{41.4}\square_{2.2}$ and $Ba_8Cd_{4.7}Ge_{40.3}\square_{1.0}$) were refined with fixed vacancy or/and Cd content in the 6d site. For all refinements anisotropic thermal

Table 3. X-ray single crystal data for $Ba_8Cd_xGe_{46-x-y}\square_y$ at $x = 2.4, 4.7, 6.5$; clathrate type I, space group $Pm\bar{3}n$; no 223 (room temperature data; redundancy > 10); standardized with program Structure Tidy [11].

	Compound[a]		
Parameter	$Ba_8Cd_{2.41}Ge_{41.36}\square_{2.23}$	$Ba_8Cd_{4.73}Ge_{40.26}\square_{1.02}$	$Ba_8Cd_{6.51}Ge_{39.06}\square_{0.43}$
Formula from refinement	$Ba_8Cd_{2.41}Ge_{41.90}\square_{2.69}$	$Ba_8Cd_{3.55}Ge_{41.45}\square_{1.00}$	$Ba_8Cd_{6.27}Ge_{39.46}\square_{0.27}$
Crystal size	$100 \times 80 \times 75\ \mu m^3$	$90 \times 90 \times 70\ \mu m^3$	$120 \times 90 \times 70\ \mu m^3$
a (nm) from single crystal	1.075 71(2)	1.085 55(2)	1.091 49(2)
a (nm), Guinier, Ge standard	1.075 18(3)	1.085 00(2)	1.091 90(2)
μ_{abs} (mm^{-1})	31.73	31.09	30.82
Data collection, 2Θ range (deg)	$2 \leqslant 2\Theta \leqslant 72.6$; 100 s/frame	$2 \leqslant 2\Theta \leqslant 72.0$; 100 s/frame	$2 \leqslant 2\Theta \leqslant 72.5$; 100 s/frame
Total number of frames	240 for 6 sets; scan width = 2°	239 for 6 sets; scan width = 2°	197 for 5 sets; scan width = 2°
Reflections in refinement (Total no of reflections)	$443 \geqslant 4\sigma(F_0)$ of 570 [2989]	$511 \geqslant 4\sigma(F_0)$ of 587 [2997]	$556 \geqslant 4\sigma(F_0)$ of 591 [2072]
Mosaicity	<0.45	<0.45	<0.40
Number of variables	21	22	19
$R_F^2 = \Sigma\lvert F_0^2 - F_c^2\rvert / \Sigma F_0^2$	0.0240	0.0213	0.025
R_{Int}	0.0399	0.0300	0.055
wR2	0.0564	0.0498	0.062
GOF	1.143	1.126	1.10
Extinction (Zachariasen)	0.0006(1)	0.0007(1)	0.0008(1)
Ba1 in 2a (0, 0, 0); occ.	1.00(1)	1.00(1)	1.00(2)
$U_{11} = U_{22} = U_{33}$ (in 10^2 nm^2)	0.0119(2)	0.0116(1)	0.0124(3)
Ba2 in 6c (1/4, 0, 1/2); occ.	1.00(1)	1.00(1)	1.00(1)
U_{11}; $U_{22} = U_{33}$	0.0231(3); 0.0420(3)	0.0233(3); 0.0424(2)	0.0208(3); 0.0402(3)
M1 in 6d (1/4, 1/2, 0); occ.	0.179(5)Ge + 0.402[b]Cd + 0.419□	0.117(3)Ge + 0.713[b]Cd + 0.17□	0.955(6)Cd + 0.045□
U_{11}; $U_{22} = U_{33}$	0.0167(5); 0.0121(4)	0.0166(3); 0.0120(2)	0.0142(3); 0.0121(2)
M2 in 16i (x, x, x); occ.	1.02(1)Ge	1.02(1)Ge	0.966(9)Ge + 0.034Cd
x:	0.183 49(3)	0.183 44(2)	0.183 53(3)
$U_{11} = U_{22} = U_{33}$; $U_{23} = U_{13} = U_{12}$	0.0144(1); −0.0025(1)	0.0126(1); −0.001 20(1)	0.0108(1); −0.0015(1)

Table 3. (Continued.)

Parameter	Compound[a]		
	$Ba_8Cd_{2.41}Ge_{41.36}\square_{2.23}$	$Ba_8Cd_{4.73}Ge_{40.26}\square_{1.02}$	$Ba_8Cd_{6.51}Ge_{39.06}\square_{0.43}$
Ge31 in 24k (0, y, z); occ.	0.329(3)Ge	0.811(3)Ge	1.01(1)Ge
y, z	0.1131(2); 0.3041(1)	0.113 37(8); 0.302 00(9)	0.114 58(5); 0.302 72(3)
U_{11}; U_{22}	0.0146(2); 0.0167(5)	0.0130(2); 0.0143(3)	0.0124(2); 0.0120(2)
U_{33}; U_{23}	0.0164(7); 0.000 03(39)	0.0126(4); −0.0012(2)	0.0132(2); 0.0007(1)
Ge32 in 24k (0, y, z); occ.	0.671(3)Ge	0.189(3)Ge	
y, z	0.1308(3); 0.3341(3)	0.1303(4); 0.3311(4)	
U_{11}; U_{22}	0.0146(2); 0.0167(5)	0.0130(2); 0.0143(3)	
U_{33}; U_{23}	0.0164(7); 0.000 03(39)	0.0126(4); −0.0012(2)	
Residual density; max; min	1.61; −1.59	1.35; −1.51	2.87; −3.45
Principal mean square	Ba1 0.0119 0.0119 0.0119	Ba1 0.0116 0.0116 0.0116	Ba1 0.0124 0.0124 0.0124
atomic	Ba2 0.0420 0.0420 0.0231	Ba2 0.0424 0.0424 0.0233	Ba2 0.0402 0.0402 0.0208
displacements, U	M1 0.0167 0.0121 0.0121	M1 0.0166 0.0120 0.0120	M1 0.0142 0.0121 0.0121
	M2 0.0170 0.0170 0.0095	M2 0.0145 0.0145 0.0087	M2 0.0122 0.0122 0.0078
	Ge3 0.0167 0.0164 0.0146	Ge3 0.0149 0.0130 0.0120	Ge3 0.0135 0.0124 0.0117
	Interatomic distances, standard deviation less than 0.0003 nm		
Ba1-8M2	0.3417	0.3447	0.3470
-12Ge31	0.3488	0.3500	0.3533
-12Ge32	0.3858	0.3861	
Ba2-8Ge32	0.3519	0.3566	
-8Ge31	0.3625	0.3672	0.3694
-4M1	0.3801	0.3836	0.3859
-8M2	0.3998	0.4035	0.4058
-4Ge32	0.4072	0.4106	
-4Ge31	0.4200	0.4233	0.4246

Table 3. (Continued.)

	Compound[a]		
Parameter	$Ba_8Cd_{2.41}Ge_{41.36}\square_{2.23}$	$Ba_8Cd_{4.73}Ge_{40.26}\square_{1.02}$	$Ba_8Cd_{6.51}Ge_{39.06}\square_{0.43}$
M1-4Ge32	0.2197	0.2246	
-4Ge31	0.2570	0.2610	0.2612
-4Ba2	0.3801	0.3836	0.3859
M2-1M2	0.2477	0.2502	0.2513
-3Ge31	0.2479	0.2489	0.2504
-3Ge32	0.2615	0.2619	
-1Ba1	0.3417	0.3447	0.3470
Ge31-1Ge32	0.0374	0.0365	
-1Ge31	0.2432	0.2460	0.2501
-1M1	0.2570	0.2610	0.2612
-2M2	0.2479	0.2489	0.2504
-1Ge32	0.2642	0.2663	
-2Ba2	0.3625	0.3672	0.3694
-1Ba1	0.3488	0.3500	0.3533
Ge32-1Ge31	0.0374	0.0365	
-1M1	0.2197	0.2246	
-2M2	0.2615	0.2619	
-1Ge31	0.2642	0.2663	
-1Ge32	0.2812	0.2828	
-2Ba2	0.3519	0.3566	

[a] Composition from EPMA; [b] Fixed variable.

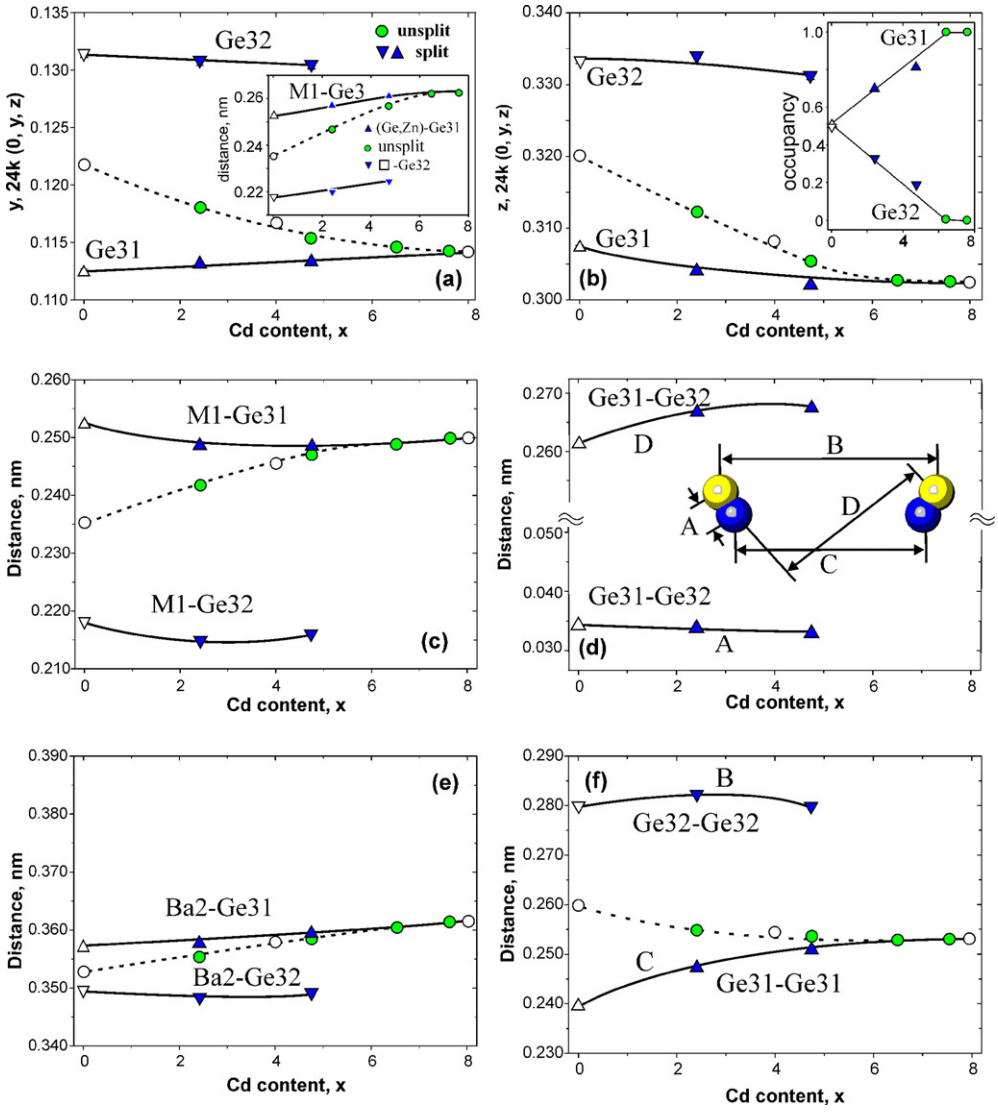

Figure 5. Compositional dependence of positional parameters for the Ge3 site (a, b) and selected interatomic distances (c, f). Filled symbols, this work; open symbols, [3] for Ba_8Ge_{43} and [6] ternary compositions.

displacement parameters (ADP) were employed. The resulting atom site distribution for all crystals $Ba_8Cd_xGe_{43-5x/8}\square_{3-3x/8}$ is summarized in figure 4.

Refinements demonstrate that incorporation of Cd atoms in the crystal lattice does not affect the 16i site ($x, x, x = 0.183\,48(5)$) whilst a significant change is observed for coordinates of the Ge3 atoms in the 24k site (figures 5(a), (b)).

Analysing the thermal atomic displacement parameters (ADPs) we encountered a large anisotropy of electron densities in two cases: (i) Ba atoms in the 6c site for all investigated single crystals and (ii) Ge atoms in 24k site (Ge3) for Cd concentrations smaller than $x = 5$. However, with increasing Cd content the anisotropy of ADPs for Ge3 decreases and finally

Table 4. X-ray single crystal data for $Ba_8Cd_{7.6}Ge_{38.4}$; clathrate-type I, space group $Pm\bar{3}n$; No. 223 (data at various temperatures; redundancy > 10). Standardized with program Structure Tidy [11].

	Temperature		
Parameter	300 K	200 K	100 K
Formula from refinement	$Ba_8Cd_{7.0}Ge_{39}$	$Ba_8Cd_{7.1}Ge_{38.9}$	$Ba_8Cd_{7.0}Ge_{39}$
Crystal size	$112 \times 84 \times 70\ \mu m^3$	$112 \times 84 \times 70\ \mu m^3$	$112 \times 84 \times 70\ \mu m^3$
a (nm)	1.095 39(2)	1.094 13(2)	1.092 87(2)
μ_{abs} (mm^{-1})	30.36	30.36	30.36
Data collection, 2Θ range (deg)	$2 \leqslant 2\Theta \leqslant 72.6$; 100 s/frame	$2 \leqslant 2\Theta \leqslant 72.0$; 100 s/frame	$2 \leqslant 2\Theta \leqslant 72.5$; 100 s/frame
Total number of frames	213 for 6 sets, scan width 2°	236 for 5 sets, scan width 2°	246 for 5 sets, scan width 2°
Reflections in refinement (Total no of reflections)	$542 \geqslant 4\sigma(F_0)$ of 604 [2120]	$511 \geqslant 4\sigma(F_0)$ of 548 [1936]	$556 \geqslant 4\sigma(F_0)$ of 591 [2072]
Mosaicity	<0.44	<0.45	<0.47
Number of variables	18	18	18
$R_F^2 = \Sigma\lvert F_0^2 - F_c^2\rvert / \Sigma F_0^2$	0.0186	0.0171	0.0195
R_{Int}	0.060	0.060	0.060
wR2	0.042	0.039	0.042
GOF	1.072	1.124	1.278
Extinction (Zachariasen)	0.0019(1)	0.0008(1)	0.0006(1)
Ba1 in 2a (0, 0, 0); occ.	1.00(1)	1.00(2)	1.00(1)
$U_{11} = U_{22} = U_{33}$ (in 10^2 nm^2)	0.0096(1)	0.006 66(1)	0.004 22(1)
Ba2 in 6c (1/4, 0, 1/2); occ.	1.00(1)	1.00(1)	1.00(1)
U_{11}; $U_{22} = U_{33}$	0.0216(2); 0.0509(2)	0.0156(2); 0.0403(2)	0.0099(2); 0.0301(2)
Cd1 (M1) in 6d (1/4, 1/2, 0); occ.	1.00(2)	1.0(2)	1.00(2)
U_{11}; $U_{22} = U_{33}$	0.0145(2); 0.0120(1)	0.0101(2); 0.0090(1)	0.0066(2); 0.0056(1)
M2 in 16i (x, x, x) ; occ.	0.937(3)Ge2 + 0.063Cd2	0.930(3)Ge2 + 0.070Cd2	0.937(3)Ge2 + 0.063Cd2
x:	0.183 47(2)	0.183 46(2)	0.183 47(2)
$U_{11} = U_{22} = U_{33}$; $U_{23} = U_{13} = U_{12}$	0.0113(1); −0.0016(1)	0.0081(1); −0.0012(1)	0.0053(1); −0.0008(1)

Table 4. (Continued.)

	Temperature		
Parameter	300 K	200 K	100 K
Ge3 in 24k (0, *y*, *z*); occ.	1.00(1)	1.00(1)	1.00(1)
y; *z*	0.114 22(3); 0.302 55(3)	0.114 28(3); 0.302 60(1)	0.114 27(3), 0.302 62(3)
U_{11}; U_{22}	0.0151(1); 0.0120(1)	0.0112(2); 0.0087(2)	0.0081(2); 0.0059(1)
U_{33}; U_{23}	0.0117(1); −0.0007(1)	0.0084(2); −0.0004(1)	0.0061(2); −0.0000(1)
Residual density; max; min	0.87; −1.27	1.37; −1.06	1.36; −1.67
Principal mean square atomic displacements *U*	Ba1 0.0096 0.0096 0.0096	Ba1 0.0067 0.0067 0.0067	Ba1 0.0042 0.0042 0.0042
	Ba2 0.0509 0.0509 0.0216	Ba2 0.0403 0.0403 0.0156	Ba2 0.0301 0.0301 0.0099
	Cd1 0.0145 0.0126 0.0126	Cd1 0.0101 0.0090 0.0090	Cd1 0.0066 0.0056 0.0056
	M2 0.0151 0.0125 0.0111	M2 0.0112 0.0090 0.0081	M2 0.0081 0.0061 0.0059
	Ge3 0.0129 0.0129 0.0082	Ge3 0.0093 0.0093 0.0058	Ge3 0.0061 0.0061 0.0038
	Interatomic distances, standard deviation less than 0.0003 nm		
Ba1-8M2	0.3481	0.3477	0.3473
-12Ge3	0.3542	0.3539	0.3535
Ba2-8Ge3	0.3707	0.3703	0.3698
-4Cd1	0.3873	0.3868	0.3864
-8M2	0.4073	0.4069	0.4064
-4Ge3	0.4265	0.4259	0.4255
Cd1-4Ge3	0.2625	0.2621	0.2618
-4Ba2	0.3873	0.3868	0.3864
M2-3Ge3	0.2513	0.2510	0.2508
-1M2	0.2524	0.2522	0.2519
-1Ba1	0.3481	0.3477	0.3473
Ge3-1Ge3	0.2502	0.2501	0.2498
-2M2	0.2513	0.2510	0.2508
-1Cd1	0.2625	0.2621	0.2618
-1Ba1	0.3542	0.3539	0.3535
-2Ba2	0.3707	0.3703	0.3698

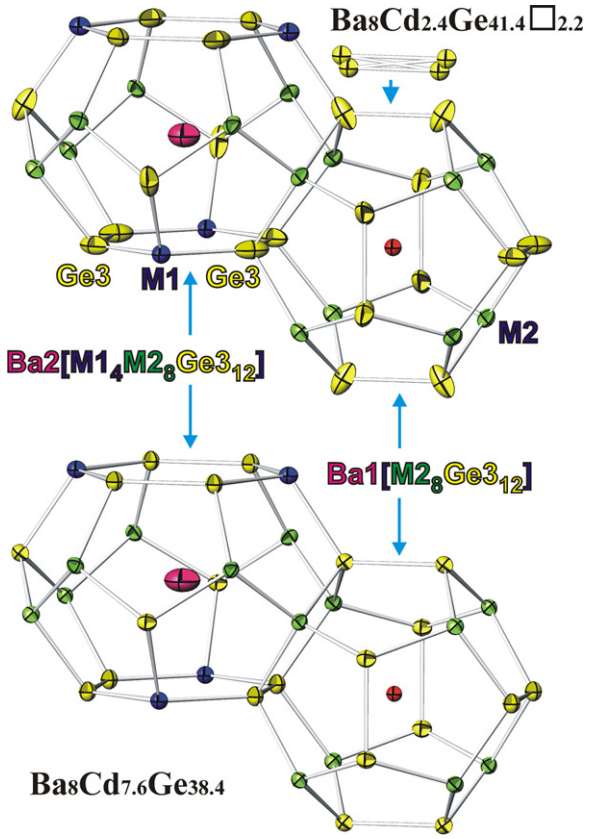

Figure 6. Cages and atom thermal displacement parameters in clathrate $Ba_8Cd_x(Ge_{43-5x/8}\square_{3-3x/8})$ (Ge3 atoms in unsplit model). The replacement of Ge3 by split Ge31 and Ge32 sites is indicated in the upper right corner.

vanishes for $x \geqslant 6$. As the direction of the ADP ellipsoids points towards the nearest neighbours in the 6d site (M1), we may associate this behaviour with vacancy formation: the three species (Ge or Cd atoms or vacancy) occupying the 6d site engage in different interactions with Ge atoms located in the 24k site and interatomic distances d_{M1-Ge3} increase in the sequence □–Ge, Ge–Ge, Cd–Ge. Accordingly the shape of the 24k site electron density adopts an ellipsoid elongated along the direction of the M-Ge3 bonds (figure 6). For binary Ba_8Ge_{43}, where only Ge atoms and vacancies share the 6d site, [4] reported a split of the 24k site into two 24k sites (Ge31 and Ge32). This possibility was carefully checked for all crystals. Indeed in refinements for $x < 6$ using split atom positions ($occ_{Ge31} + occ_{Ge32} = 1$) reliability factors decrease from about 4 to 2.5% and residual electron densities from 5 to less than 1.6 e/Å^3, yielding featureless difference-Fourier maps $F_{obs} - F_{calc}$. The results of the refinement are listed in tables 3 and 4. Three facts have to be emphasized when describing the Ge3 sites:

(i) as seen from the inset in figure 5(b), the population of Ge31 increases with increasing Cd content from ∼50% in $BaGe_{43}$ to a full occupation for $x > 6$;

(ii) consequently y and z parameters of Ge31 approach the values of the unsplit model for $x > 6$ (see figures 5(a), (b));

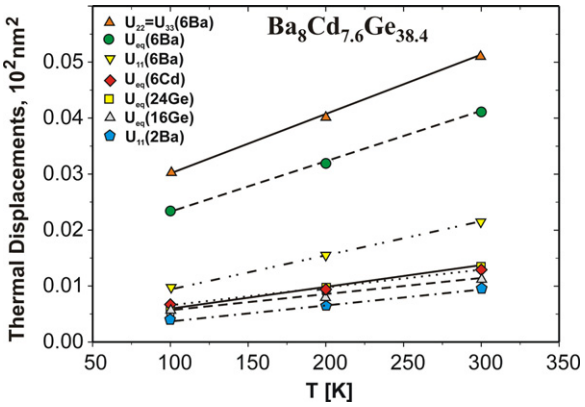

Figure 7. Thermal displacement parameter of $Ba_8Cd_{7.6}Ge_{38.4}$ versus temperature.

(iii) the internal distance $d_{Ge31-Ge32}$ stays constant (0.035 nm) for all crystals where split sites were used (distance A, see figure 5(d)).

The changes in the Ge3 sites seem to be correlated with changes in the 6d site: the decrease in the number of vacancies in the 6d site with simultaneous increase of Cd content results in a decrement of the anisotropy of ADPs for the 24k sites. For almost complete occupation of the 6d site by Cd atoms, the electron density centred at 24k finally adopts a regular shape (see tables 3, 4).

The change of the crystallographic parameters (lattice parameter, atomic coordinates and site occupancy) with Ge/Cd substitution is well reflected by a compositional dependence of the interatomic distances (tables 2 and 3).

The ADP parameters for Ba atoms located in the 6c site (Ba2) show significant anisotropy in contrast to Ba1 atoms in site 2a, which seem to have normal behaviour (tables 3 and 4). Coordination polyhedra for both barium atoms are shown in figure 6. If the $Ba_8Cd_{7.6}Ge_{38.4}$ crystal is considered as a simple Debye solid and additionally with Ba2 atoms behaving like Einstein oscillators, the thermal displacements and the Einstein temperatures $\Theta_{E,ii}$ are related by

$$U_{ii} = \frac{\hbar^2}{2m_{Ba}k_B\Theta_{E,ii}} \coth\left(\frac{\Theta_{E,ii}}{2T}\right),$$

where m_{Ba} is the atomic mass of Ba. From the linear slope $\Delta U_{ii}/\Delta T$ in figure 7 the force constants, $K_{ii} = 4\pi^2 m \nu_{ii,Ba}^2$ (g s^{-2}), the frequency of vibrations ν_{ii} (10^{12} s^{-1}), and hence the Einstein temperatures, $\Theta_{E,ii}$ (K), can be extracted. From symmetry constraints U_{11} is different from $U_{22} = U_{33}$, yielding $\Theta_{E,11} = 78$ K and $\Theta_{E,22} = 58$ K in line with the flat rotational ellipsoid of Ba2 atoms squeezed between the two hexagons of the framework tetrakaidecahedron (see figure 6). It is interesting to note that Ba1 atoms in the smaller pentagondodecahedral cage do not show a thermal displacement factor (spherical by symmetry) enhanced over the general ADP values for framework atoms. Thus no special rattling effect can be expected from Ba1 atoms.

3.3. Physical properties

3.3.1. Temperature dependent heat capacity. Specific heat measurements were performed on the clathrate having the highest content of Cd, i.e. $Ba_8Cd_{7.6}Ge_{38.4}$. Results of this investigation

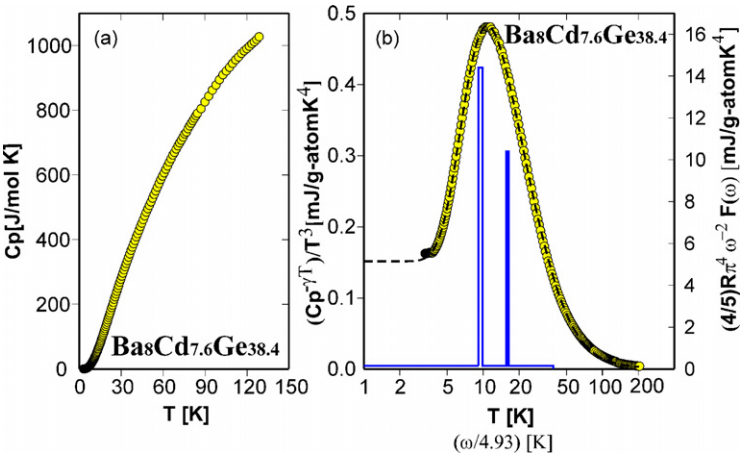

Figure 8. Temperature dependent specific heat C_p of $Ba_8Cd_{7.6}Ge_{38.4}$, plotted as C_p versus T (a) and $(C_p{-}\gamma T)/T^3$ versus T (b). The dashed line is a least squares fit of the experimental data using the model described in the text. The essential parameters of the model used to construct the spectral function $F(\omega)$ (solid lines, right axis) are $\theta_D = 192$ K, $\theta_{E1} = 46 \pm 2$ K and $\theta_{E2} = 78.5 \pm 1.6$ K.

are displayed in figures 8(a) and (b). The heat capacity at low temperature ($T < 4$ K) can be described in terms of an electronic contribution $\gamma = 2$ mJ mol^{-1} K^{-2} and a lattice contribution $\beta = 0.008\,44$ J mol^{-1} K^{-4}, yielding a low temperature Debye temperature $\theta_D^{LT} = 230$ K. This standard description, however, already breaks down above about 4 K, referring to a rather complicated phonon spectrum due to the distinct crystal structure of $Ba_8Cd_{7.6}Ge_{38.4}$, filled by the electropositive element Ba. Moreover, the complete Debye function is unable to also account for the temperature dependent specific heat of $Ba_8Cd_{7.6}Ge_{38.4}$ in an extended temperature range. In order to gain more insight into the lattice dynamics, we have adapted a specific heat model using a more structured phonon density of states [12, 13]. The latter is represented by a spectral function $F(\omega)$ introduced by Chambers [14]. The heat capacity can then be modelled by:

$$C_{ph}(T) = 3R \int_0^\infty F(\omega) \frac{(\frac{\omega}{2T})^2}{\sinh^2(\frac{\omega}{2T})} d\omega, \tag{1}$$

with R the gas constant and ω the phonon frequency. In order to obtain the heat capacity in standard units, $F(\omega)$ has to be normalized to the number of branches of the dispersion relation, i.e. $3n$ for n atoms in the unit cell. The most common assumptions on $F(\omega)$ are $F(\omega) = \delta(\omega)$ and $F(\omega) \sim \omega^2$ up to a cut-off frequency ω_D, corresponding to the well known Einstein and Debye model, respectively. The approach of Junod *et al* consists of a ω^2 dependence with different pre-factors for the different frequency regions. The phonon density vanishes for $\omega > \omega_D$. To fulfil the normalization condition concerning the number of phonon branches, the following equation applies:

$$\int_0^\infty F(\omega)\, d\omega = 3 \times 54 \tag{2}$$

since the crystalline unit cell consists of 54 atoms. It has been shown that certain functionals of the phonon specific heat take the form of convolutions of the phonon spectrum. In particular, $(5/4)R\pi^4 C_{ph} T^3$ is an image of the spectrum $\omega^{-2}F(\omega)$ for $\omega = 4.93T$, where ω is expressed in kelvin. Based on these considerations, a simple phonon spectrum is constructed to account for the temperature dependent specific heat. Results are shown in figure 8. The Sommerfeld

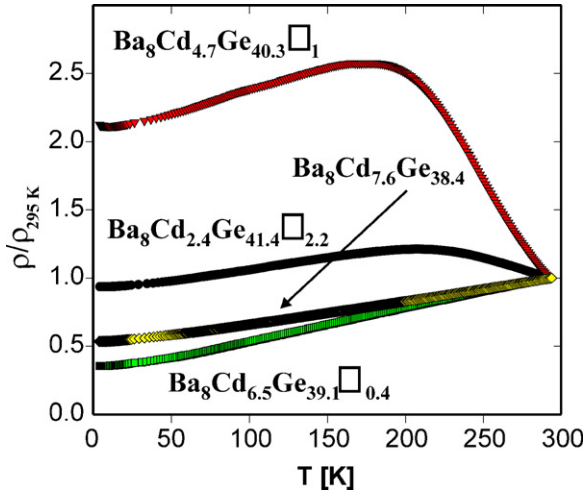

Figure 9. Temperature dependent normalized resistivity $\rho/\rho_{295\ \mathrm{K}}$ of $Ba_8Cd_xGe_{43-5x/8}\square_{3-3x/8}$.

value γ is subtracted, thus the experimental points in figure 8 refer to the phonon contribution only. A proper description of the temperature dependent specific heat is obtained employing a Debye temperature $\theta_D = 192$ K and two Einstein-like contributions, $\theta_{EL1} = 46$ and $\theta_{EL2} = 78.5$ K, with corresponding spectral widths of 4 and 3.2 K, respectively. Accordingly, both contributions have different spectral weights. The analysis provided evidence that besides a simple Debye approach, two Einstein branches have to be added in order to account for the spectrum of lattice vibrations present in $Ba_8Cd_{7.6}Ge_{38.4}$, at least at lower temperatures. Adding these additional branches means accounting for very localized phonon branches. At first sight the cage like structure formed by the (Cd, Ge) network may constitute the background Debye-like spectrum, while the electropositive element Ba, which fills the oversized cages, gives rise to rattling modes, represented by two Einstein branches. Here, it should be noted that the Einstein contribution is not a δ-function, rather, it replenishes a temperature width of a few kelvin. However, when comparing this type of analysis with data available for skutterudites [15], a much narrower temperature range for the Einstein branches is obtained for clathrates.

Localized lattice vibrations were also derived from the XRD analysis of the anisotropic thermal displacement factor of Ba2 yielding two Einstein temperatures, whilst no distinct vibrational modes were deduced for Ba1. Although treatment of the temperature dependent specific heat coincides with the Einstein temperatures obtained from the ADPs, a 1:1 correspondence between both sets of temperatures may be somehow artificial. Assuming that the smaller Einstein temperature belongs to the Ba2 sites, the cage structure around Ba2 and its elastic deformation may then give rise to a further Einstein mode, $\theta_{EL2} = 78.5 \pm 1.6$ K.

3.3.2. Temperature dependent transport. Materials under investigation are characterized by their proximity to a metal-to-insulator transition because of a significantly reduced charge carrier concentration. As a result, the overall resistivities are quite large, exceeding those of typical intermetallic compounds by more than one order of magnitude (see figure 9). The room temperature resistivities are 8322, 10 330, 401 and 453 $\mu\Omega$ cm for the $Ba_8Cd_xGe_{46-x-y}\square_y$, $x = 2.4$, 4.7, 6.5 and 7.6 samples, respectively.

$BaCd_xGe_{46-x-y}\square_y$, $x = 6.5$ and 7.6 exhibit metallic like behaviour, i.e. $\rho(T)$ increases steadily with increasing temperature; however, particular features in $\rho(T)$ do not follow a simple temperature dependence originating from scattering of charge carriers (electrons or

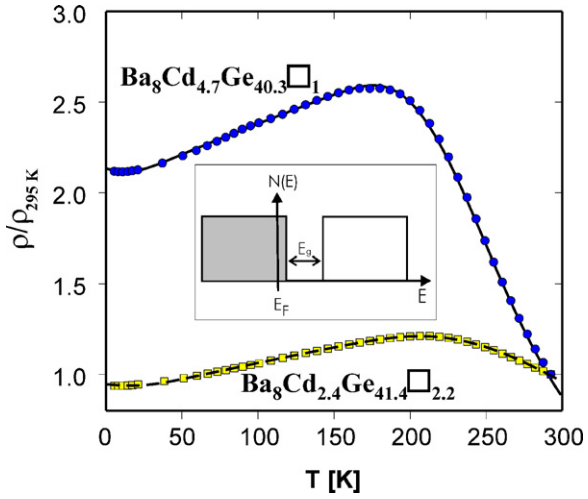

Figure 10. Normalized electrical resistivity ρ of $Ba_8Cd_{2.4}Ge_{41.4}\square_{2.2}$ and $Ba_8Cd_{4.7}Ge_{40.3}\square_{1.0}$. The solid lines are least squares fits explained in the text. The inset is a sketch of the electronic density of states model in the vicinity of the Fermi energy E_F.

holes) on thermally excited phonons. The latter is usually expressed by the Bloch–Grüneisen formula,

$$\rho_{\mathrm{ph}} = \frac{C}{\Theta_D}\left(\frac{T}{\Theta_D}\right)^5 \int_0^{\Theta_D/T} \frac{z^5\,\mathrm{d}z}{(\mathrm{e}^z-1)(1-\mathrm{e}^{-z})} \tag{3}$$

where C is a temperature independent electron–phonon interaction constant and Θ_D is the Debye temperature. Equation (3) causes a T^5 behaviour of $\rho(T)$ at low temperatures ($T \ll \Theta_D$), whilst at elevated temperatures $\rho(T)$ should behave linearly. A closer inspection of the data of figure 9 shows that at low temperatures $\rho(T)$ roughly follows a $T^{2.5}$ dependence, which can never be reproduced by applying equation (3). Moreover, the tendency of the data towards a positive slope, i.e. $\mathrm{d}\rho/\mathrm{d}T > 1$, is not accounted for in terms of equation (3).

Deviations from the Bloch–Grüneisen behaviour become even worse if the number of charge carriers is changed, varying the Cd content (figure 9). Here, $\rho(T)$ evidences a crossover from a metallic-like behaviour for large Cd contents to a more complex temperature dependence for $x = 2.4$ and 4.7. Around room temperature both the latter compounds exhibit a semiconducting-like temperature dependence of $\rho(T)$, while below a maximum, a metallic like behaviour becomes obvious. Additionally, a small upturn of $\rho(T)$ can be observed for $T < 10$ K. In order to get rid of those rather uncommon features, we have developed a model [15], which combines the description of simple metals via the Bloch–Grüneisen law with a temperature dependent charge carrier density. The latter follows from distinct features of the electronic density of states (DOS) around the Fermi energy E_F. To simplify the calculations, we have assumed that the DOS can be represented by rectangular bands. The proximity of the present systems to isolating states has to be reflected by a gap in the DOS slightly above E_F having an appropriate width E_g (compare the inset in figure 10). These assumptions allow us to calculate both the density of electrons, n_n, and the density of holes, n_p, using standard statistics and involving the Fermi–Dirac distribution function $f(E, T)$. Considering this rectangular density of states model, $N(E)$, n_n follows from

$$n_n(T) = \int_{E_F}^{\infty} N(E)\, f(E,T)\,\mathrm{d}E \tag{4}$$

as

$$n_n(T) = -NE_g + Nk_BT \ln\left(1 + \exp\left(\frac{E_g}{k_BT}\right)\right) \tag{5}$$

where N is the band height. With similar arguments, the hole density n_p can be derived:

$$n_p(T) = \int_{-\infty}^{E_F} N(E)(1 - f(E,T))\,\mathrm{d}E \tag{6}$$

revealing

$$n_p(T) = -Nk_BT \ln 2. \tag{7}$$

The total charge carrier density $n(T)$ is then simply given by

$$n(T) = \sqrt{n_n(T)n_p(T)} + n_0 \tag{8}$$

where n_0 is a residual density of states, accounting for the fact that at $T = 0$ the samples investigated exhibit finite residual resistivity. Finally, the overall resistivity of such systems can be expressed as

$$\rho(T) = \frac{\rho_0 n_0 + \rho_{ph}}{n(T)} \tag{9}$$

where ρ_0 is the residual resistivity and ρ_{ph} is given by equation (3).

A least squares fit to the data of figure 9 was carried out considering equation (9). Results of such a procedure are plotted in figure 10 as solid lines. Despite of the fact that the model is simple, the results describe astonishingly well the experimentally derived temperature dependences. The most important parameter appears to be the gap width E_g, which for $Ba_8Cd_{2.4}Ge_{41.4}\square_{2.2}$ and $Ba_8Cd_{4.7}Ge_{40.3}\square_{1.0}$ amounts to 2570 and 3230 K, respectively. Besides other features in $\rho(T)$ within the model outlined, a very narrow region of the DOS right above E_F, also defining the gap distance from E_F, is responsible for the metallic $\rho(T)$ dependence of the present clathrates at lower temperatures. Note also that features like a small upturn in $\rho(T)$ at the lowest temperatures are quite well reproduced too.

The temperature dependent thermal conductivity, λ, of $Ba_8Cd_xGe_{43-5x/8}\square_{3-3x/8}$ is displayed in figure 11(a) for the temperature range from 4 K to room temperature. As expected for clathrates, overall $\lambda(T)$ values are small and are dominated by the lattice thermal conductivity λ_l at low temperatures. An analysis of the data relies on the Wiedemann–Franz law, which, to a first approximation, allows us to split the measured thermal conductivity into an electronic part, λ_e, and a lattice part, λ_l. The lattice thermal conductivity (see figure 11(b)) derived in this approximation shows very small values at medium temperatures, thereby evidencing an important interaction process that substantially lowers λ_l: scattering of the phonons on charge carriers (compare equation (11), with $\square_E^{-1} = E\omega$, E being a constant and ω the phonon frequency). In fact the compounds richest in Cd exhibit the lowest lattice thermal conductivity. This is referred to the previously indicated mechanism since the compounds $Ba_8Cd_{7.6}Ge_{38.4}$ and $Ba_8Cd_{6.5}Ge_{39.1}\square_{0.4}$ show the least resistivity, giving rise to an enhanced interaction of the heat-carrying phonons with the conduction electron system. On the other hand, the $Ba_8Cd_{4.7}Ge_{40.3}\square_{1.0}$ compound exhibits an almost doubled lattice thermal conductivity around 150 K. This coincides with the largest overall electrical resistivity of the present series. One can then conclude that the reduced charge carrier density and/or smaller mobility yields only to weak interactions of both phonons and the charge carriers. Hence, the lattice thermal conductivity remains relatively large. To further analyse the present data we have adopted Callaway's model to account for the lattice thermal conductivity [16], using the standard notation:

$$\lambda_l = CT^3 \int_0^{\theta_D/T} \frac{\tau_C x^4 \exp(x)}{[\exp(x) - 1]^2}\,\mathrm{d}x \tag{10}$$

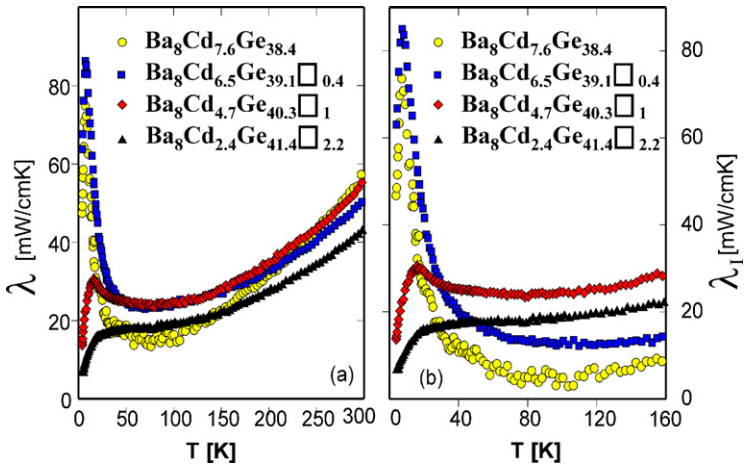

Figure 11. (a) Temperature dependent thermal conductivity λ of $Ba_8Cd_xGe_{43-5x/8}\square_{3-3x/8}$ with $x = 2.4, 4.7, 6.5, 7.6$. (b) Temperature dependent lattice thermal conductivity λ_l for the same samples.

where τ_c represents the overall relaxation time for scattering processes, C is a constant and θ_D is the Debye temperature. Taking into account the most relevant scattering processes present in the clathrates investigated, the relaxation time can be expressed as:

$$\tau_C^{-1} = \tau_B^{-1} + \tau_D^{-1} + \tau_U^{-1} + \tau_E^{-1} \tag{11}$$

where the subscripts B, D, U and E refer to scattering processes of the heat-carrying phonons with boundaries, dislocations, Umklapp processes, resonance scattering and electrons, respectively. Additionally, a T^3 term was added in order to get rid of the radiation losses, according to the steady state heat flow method used.

Results of least squares fits are shown as solid and dashed lines in figure 12, where the dashed line corresponds to the T^3 correction. The low temperature slope of $\lambda_\ell(T)$ follows from a balance of boundary and point defect scattering; it becomes large when both quantities are small. Umklapp scattering effectuates a decrease of $\lambda_\ell(T)$ above a certain temperature, thereby forming a maximum in $\lambda_\ell(T)$ at lower temperatures. This maximum depends weakly on the Debye temperature and occurs well below $\Theta_D/10$. An increase of Θ_D slightly reduces the overall $\lambda_\ell(T)$ values. The experimentally observed fact that an increase in the Cd content enhances the low temperature maximum in $\lambda_\ell(T)$ (compare figure 11(b)) would refer to a lowering of boundary and/or point defect scattering. Although the Ge/Cd substitution creates increasing statistical disorder, the replenishing of the vacancies is made responsible for this observed low temperature feature.

Figure 12 also demonstrates that the lattice thermal conductivity of $Ba_8Cd_{7.6}Ge_{38.4}$ is near to the theoretical limit of thermal conductivity, a necessity for thermoelectric applications of such materials. According to Cahill and Pohl [17], the theoretical lower limit of the lattice thermal conductivity is primarily defined by the number of atoms per unit volume and by the Debye temperature. Taking $n = 4.11 \times 10^{28}$ m^{-3}, two curves are calculated for $\theta_D = 192$ and 230 K, respectively. Results are shown in figure 12 as dashed–dot and dashed-dot–dot lines, respectively, revealing λ_{min} (300 K, $\theta_D = 192$ K) $= 3.65$ mW cm^{-1} K^{-1} and λ_{min} (300 K, $\theta_D = 230$ K) $= 4.34$ mW cm^{-1} K^{-1}. In fact, these calculations demonstrate that the lattice thermal conductivity of $Ba_8Cd_{7.6}Ge_{38.4}$ at elevated temperatures is in the proximity of the theoretical minimum. This refers to the fact that at least $Ba_8Cd_{7.6}Ge_{38.4}$ behaves within the concept of a phonon glass.

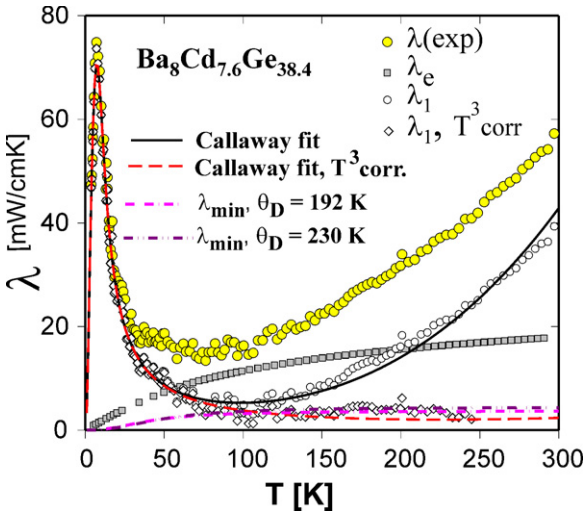

Figure 12. Temperature dependent thermal conductivity λ of $Ba_8Cd_{7.6}Ge_{38.4}$ (large circles). The electronic λ_e (filled small squares) and the lattice contribution λ_l (filled small circles) are derived from the Wiedemann–Franz law. The small diamonds represent the lattice contribution corrected for radiation losses. The solid and the dashed lines are least squares fits applying the model of Callaway with and without a T^3 term for radiation losses. The dashed–dot and the dashed–dot–dot lines are calculations of the theoretical lower limit of thermal conductivity for $\theta_D = 192$ K and $\theta_D = 230$ K, respectively.

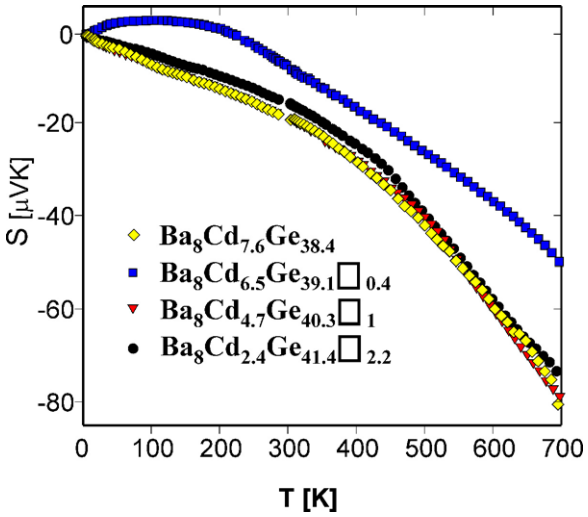

Figure 13. Temperature dependent thermopower of $Ba_8Cd_xGe_{43-5x/8}\square_{3-3x/8}$ with $x = 2.4$, 4.7, 6.5, 7.6.

Measurements of the temperature dependent thermopower, S, are shown in figure 13 for $Ba_8M_xGe_{43-5x/8}\square_{3-3x/8}$ with M = Cu, Zn, Cd. All systems displayed have in common negative thermopower values referring to electrons as majority charge carriers. Moreover, $S(T)$ does not exhibit much structure in its temperature dependence, evidencing electronic transport without significant correlations within the system of charge carriers. This absence also follows from the Sommerfeld value of the specific heat being as low as 2 mJ mol^{-1} K^{-2}. Moreover, the

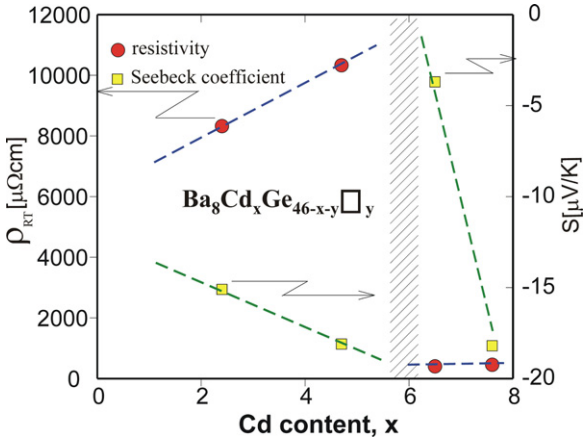

Figure 14. Concentration dependence of the resistivity ρ (circles) and of the Seebeck coefficient S (square symbols) at room temperature (RT).

moderate thermopower values of the present family of clathrates may also follow from a rather weak energy dependence of the DOS right at E_F. This, in turn, somehow justifies the use of a simple DOS as considered for the analysis of the temperature dependent resistivity.

Figure 14 shows the concentration dependent variation of the room temperature resistivity and of the Seebeck coefficient. Both quantities are characterized by a significant variation around a Cd content of six Cd atoms per formula unit. These abrupt changes correlate well with the filling of the 6d site by Cd atoms, simultaneously reducing the vacancy concentration. Above a Cd content of six, Cd subsequently enters the 16i sites. This distinct substitution mechanism obviously changes details of the electronic density of states at the Fermi level, thereby altering electronic transport such as resistivity and the Seebeck coefficient.

4. Summary

We have prepared a number of clathrates based on the parent compound Ba_8Ge_{43}. The substitution of Ge by Cd allows a variation of the charge carrier density, hence transport quantities like the electrical resistivity, thermal conductivity and thermopower are influenced in a very distinct manner. In particular such systems may be driven towards a metal to insulator transition, as obvious from the temperature dependent resistivity of $Ba_8Cd_xGe_{43-5x/8}\square_{3-3x/8}$ for $2.4 \leqslant x \leqslant 7.6$. We have developed a model density of states, characterized by a narrow gap of the DOS right above the Fermi energy, which allows us to qualitatively trace various details of the temperature dependent electrical resistivity. Thermal conductivity data are modelled within the standard Callaway theory of heat-carrying phonons. Measurements of the Seebeck coefficient allowed us to test these materials with respect to thermoelectric applications. Combining our experimental data to derive the figure of merit $ZT = S^2/(\rho\lambda)$ at room temperature as a measure of thermoelectric performance, we arrive at $ZT(300\ \mathrm{K}) = 0.0042$ for $Ba_8Cd_{7.6}Ge_{38.4}$. This value, however, neglects the correction of radiation losses, which, when applied, renders $ZT_{\mathrm{corr}}(300\ \mathrm{K}) = 0.013$. Using the experimental thermopower data at 700 K in combination with careful extrapolation of resistivity (ρ (700 K) $\approx$ 775 $\mu\Omega$ cm) and of thermal conductivity (λ_{corr} (700 K) $\approx$ 30 mW cm^{-1} K^{-1}) we obtain $ZT_{\mathrm{corr}}(700\ \mathrm{K}) = 0.192$. Applications are possible if the thermoelectric figure of merit surpasses a value of $ZT = 1$ as realized in Bi_2Te_3 with $ZT(300\ \mathrm{K}) \approx 0.7$ [18].

Acknowledgments

The research reported herein was supported by the Austrian FWF project P16370, P16778-No2 and P19165. NM-K and PR are both grateful to the OEAD Austrian–Ukrainian Scientific Technological Exchange Program 'Ernst Mach' for fellowship in Wien.

References

[1] Rowe D M (ed) 1995 *CRC Handbook of Thermoelectrics* (Boca Raton, FL: CRC Press)
[2] Nolas G, Slack G, Morelli D T, Tritt T M and Ehrlich A C 1996 *J. Appl. Phys.* **79** 4002
[3] Carrillo-Cabrera W, Curda J, Petters K, Baenitz M, Grin Y and von Schnering H G 2000 *Z. Krist. New Cryst. Struct.* **215** 321
[4] Carrillo-Cabrera W, Budnyk S, Prots Y and Grin Y 2004 *Z. Anorg. Allg. Chem.* **630** 7226
[5] Czybulka A, Kuhl B and Schuster H U 1991 *Z. Anorg. Allg. Chem.* **594** 23
[6] Kuhl B, Czybulka A and Schuster H U 1995 *Z. Anorg. Allg. Chem.* **621** 1
[7] Carrillo-Cabrera W, Borrmann H, Paschen S, Baenitz M, Steglich F and Grin Y 2005 *J. Solid State Chem.* **178** 715
[8] Nonius Kappa CCD 1998 *Program Package COLLECT, DENZO, SCALEPACK, SORTAV* (The Netherlands: Nonius Delft)
[9] Sheldrick G M 1997 *SHELXL-97, Program for Crystal Structure Refinement* (Germany: University of Göttingen) (Windows version by McArdle, Natl. Univ. Ireland, Galway)
[10] Roisnel T and Rodriguez-Carvajal J 2001 *Mater. Sci. Forum* **378–381** 118
[11] Parthé E, Gelato L, Chabot B, Penzo M, Cenzual K and Gladyshevskii R 1994 *TYPIX Standardized Data and Crystal Chemical Characterization of Inorganic Structure Types* (Berlin: Springer)
[12] Junod A, Bichsel D and Muller J 1979 *Helv. Phys. Acta* **52** 580
[13] Junod A, Jarlborg T and Muller J 1983 *Phys. Rev.* B **27** 1568
[14] Chambers R G 1961 *Proc. Phys. Soc. Lond.* **78** 941
[15] Berger St 2003 *PhD Thesis* Vienna University of Technology
[16] Callaway J and von Baeyer H C 1960 *Phys. Rev.* **120** 1149
[17] Cahil D and Pohl R 1989 *Solid State Commun.* **70** 927
[18] Tritt T 1999 *Science* **283** 804